Mon. Not. R. astr. Soc. (1970) **147**, 215–230.

A HIGH-RESOLUTION MAP OF CASSIOPEIA A AT 2·7 GHz

Ivan Rosenberg

(Communicated by P. A. G. Scheuer)

(Received 1969 October 30)

SUMMARY

Observations of Cas A (3C 461) have been made using the Cambridge One-mile telescope at a frequency of 2695 MHz with a beamwidth of 12″ × 14″ arc. The high resolution has revealed complex structure in the source and some of the spurs observed previously at a lower resolution have been found to be separated compact components of high emissivity. By comparing the new observations with earlier ones made at 1407 MHz variations of structure with frequency across the source have been found, with spectral indices higher on average on the west half of the source than on the east. Comparisons with optical photographs show a remarkable correlation between the gaps in the radio shell and some of the high velocity optical filaments. Estimates of some physical parameters of the main source and of the compact components are derived in the last part of the paper.

1. INTRODUCTION

Cassiopeia A (3C 461), situated at $l^{II} = 111{\cdot}7°$, $b^{II} = 2{\cdot}1°$ and at 3·4 kpc from the Sun, is thought to be the remnant of a type II supernova of about 300 years ago (e.g. Minkowski 1968, van den Bergh & Dodd 1969). At radio wavelengths, the most detailed map yet published is that by Ryle, Elsmore & Neville (1965) with a resolution of 23″ arc at 1407 MHz. This map shows that the source has a circular ring of emission with an angular diameter of about 4′ arc, but that the emission around the ring is by no means uniform. Complex structure was detected within the ring, which is presumably the projection of a three-dimensional shell.

These features have been confirmed by other observations of somewhat lower resolution, such as those of Mayer & Hollinger (1968) at 19 GHz with a resolution of 102″ arc, Hobbs, Corbert & Santini (1968) at 31 GHz with 96″ arc resolution, and Braun & Yen (1968) at 35 GHz with a resolution of 60″ arc, among others.

Polarized emission has also been detected from the source, the most remarkable observations being those of Mayer & Hollinger (1968) who found linear polarization of about 4 per cent to 7 per cent around the circumference of the source with a high degree of circular symmetry. Weak linear polarization (one per cent or less) has also been detected at 14·5 GHz by Hobbs & Hollinger (1968), at 8·35 GHz by Hollinger & Hobbs (1968), at 8·0 GHz by Hobbs and Haddock (1967) and at 1408 MHz by Seielstad & Weiler (1968).

This paper presents a map, obtained at 2695 MHz, which has a higher resolution than any previously published map of the source. The observations are described in Section 2 and the results in Section 3. Estimates of the physical characteristics of the bulk of the source are derived in Section 4 and a discussion on some compact components revealed by these observations is given in Section 5.

2. OBSERVATIONS

The source was observed during the period 1968 October–December using the Cambridge One-mile telescope (Ryle 1962), the method of operation of which has been fully described elsewhere (Elsmore, Kenderdine & Ryle 1966).

The telescope synthesizes an aperture consisting of equally spaced concentric annuli lying in the equatorial plane; 32 spacings of the aerials were used for these observations. The aperture illumination was graded with a function which falls to 30 per cent at the edge of the aperture. The resulting reception pattern has a width between half-power points of 12″ arc in R.A. and 12″ cosec δ arc (i.e. 14″ arc) in declination, and a first sidelobe response of 5 per cent. The first grating response has a radius of about 500″ arc which is twice the diameter of the source. The feeds of the three aerials were set parallel to each other and aligned at position angle 0° throughout the observations; thus only one component of linear polarization was accepted. Preliminary measurements of polarization indicated, however, that no part of the source is strongly polarized at this frequency and an upper limit of 2 per cent could be set to the polarization of the major features. The structure revealed in the present map will not, therefore, differ significantly from the true distribution of total emission.

Calibrations for every spacing were made to determine the sensitivity and the collimation error of the telescope, using the point sources 3C 147, 3C 309·1 and 3C 295 with adopted flux densities of 13·0, 5·3 and $11{\cdot}9\times10^{-26}$ W m^{-2} Hz^{-1} respectively. As a check on the calibrations the total flux of the source was estimated and the result was found to be in agreement, within the limits of error, with the value derived from the spectrum (Parker 1968) based on absolute measurements.

The observational data were processed with the help of the TITAN computer of the Cambridge University Mathematical Laboratory, giving a contour map of the brightness distribution as the final output.

3. RESULTS

3.1 *General features*

A contour map of the source is shown in Fig. 1 and also in Plate I superimposed on a recent photograph of the optical filaments taken with the 200-inch Palomar Telescope (van den Bergh, private communication). The contour interval is 1260°K in brightness temperature.

It can be seen from the map that, although the source is circular in outline, the brightness distribution within it is highly irregular and shows numerous peaks of enhanced emission and some gaps in the main shell structure. Shell-type radio sources with irregular features have been observed by Hill (1967) and Kesteven (1968), among others. The following features may be noted:

3.1.1 A total of 25 peaks of enhanced emission are clearly visible and are identified by crosses in Fig. 1. Peaks near the edge of the source seem brighter in general than those near the centre by a factor of two or more, even when allowance is made for an underlying shell; the smaller angular diameter of those seen near the edge suggests that the emitting regions are not spherically symmetrical, but are flattened in the direction of expansion.

3.1.2 Three of these emission regions appear outside the main shell and are clearly separated from it. They are labelled I, II and III in Fig. 3. Their positions, flux densities and angular sizes are shown in Table I. Indications of

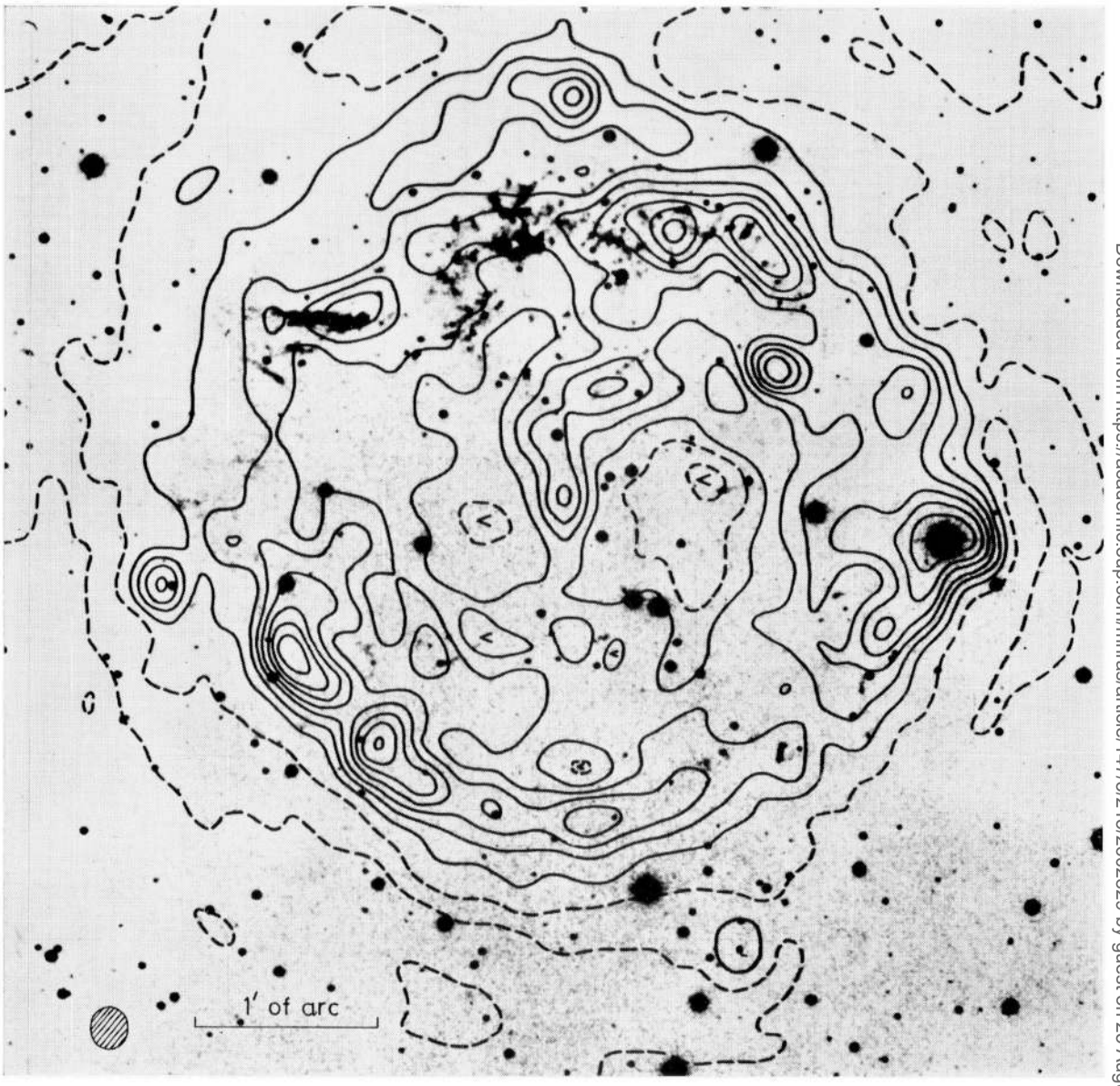

PLATE I

Mt Wilson and Palomar Observatory photograph of Cas A, courtesy of S. van den Bergh, taken in Autumn 1968. *The* 2695 *MHz contour map is superimposed. The half-power beamwidth of the radio telescope* (12″ × 14″ *arc*) *is also shown. Isolated minima are indicated by the symbol* <.

[*facing p.* 216]

1970MNRAS.147..215R

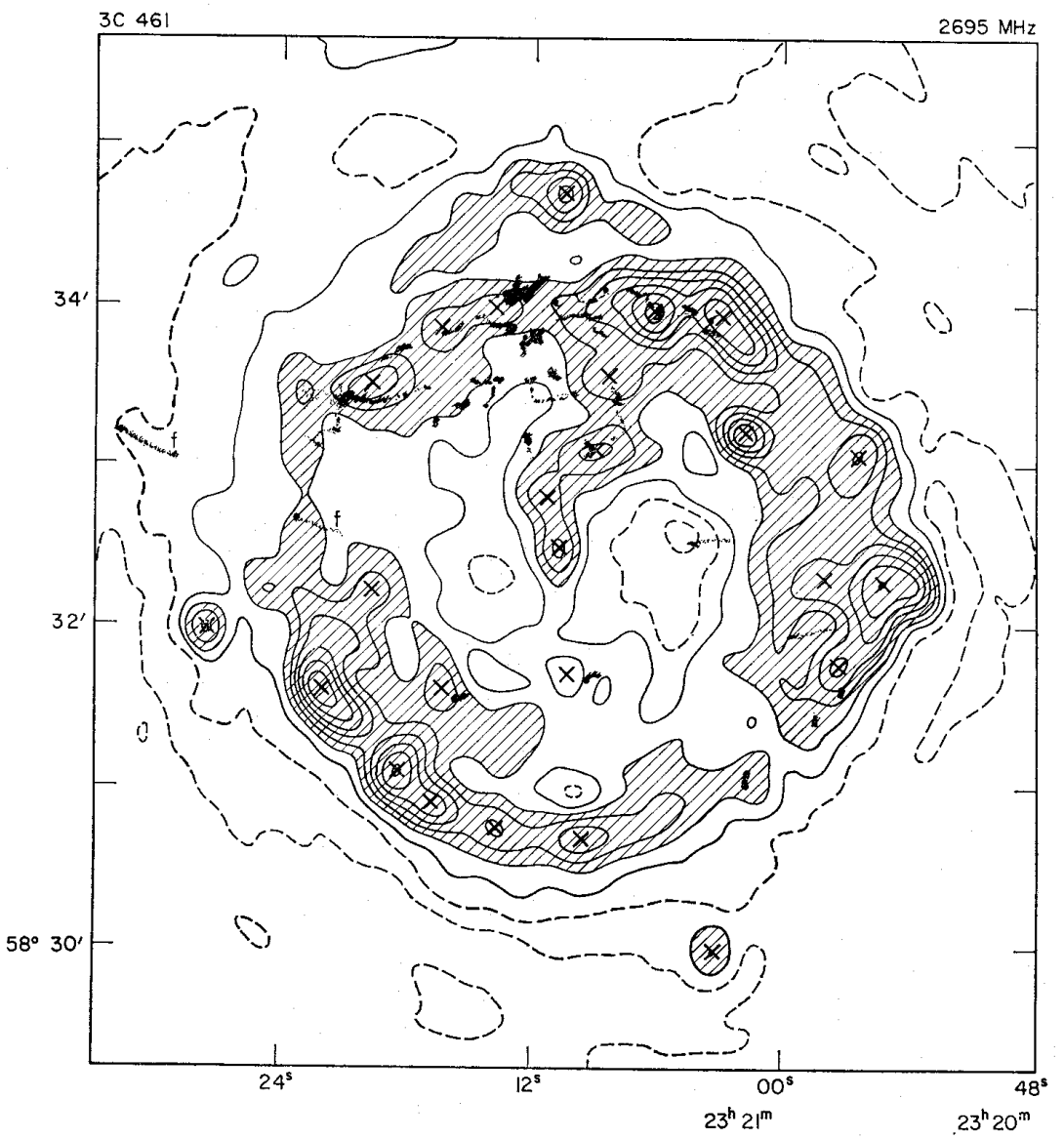

FIG. 1. *Contours of Cas A at 2695 MHz. Coordinates are for epoch 1950.0. The contour interval is 1260°K. The first dashed contour represents the zero contour. Shaded filaments are reproduced from the 200-inch photograph of Baade & Minkowski (1954). The symbols × indicate the 25 peaks of emission.*

these regions may be found in the spurs on the 1407 MHz map by Ryle *et al.* (1965). By comparing the two maps (see below), spectral indices for these sources may be estimated and the results are also shown in Table I. There is a very high probability that these regions are associated with the supernova remnant; the probability of finding by chance even a single source as bright or brighter in the field covered by the map (4×10^{-6} sr) has been estimated by extrapolating their fluxes determined from 2695 MHz and 1407 MHz data to 408 MHz and using the log N–log S curves of Pooley & Ryle (1968). It is of the order of 10^{-5}. These three regions are discussed further in Section 5.

3.1.3 As was found at 1407 MHz, there appears to be a plateau of low surface brightness which extends beyond the apparent edge of the source defined by the shell. This more extended region reaches as far out as the three compact components mentioned above.

3.1.4 The central part of the source is less bright than would be expected from a uniform and isotropically emitting shell model fitted to the outer rim emission (see Section 4.2). This phenomenon has also been observed in other supernova remnants, 3C 10 (Tycho's Nova) (Baldwin 1967), W 49B (Wynn-Williams 1969) and in the southern hemisphere by Whiteoak & Gardner (1968) and Kesteven (1968), among others.

3.1.5 There are two notable gaps in the ring which seem to be part of a band of reduced emission running across the source at about position angle 70° and slightly below the centre of the shell.

TABLE I

	Position (1950.0)	Spectral index α	S_{2695} 10^{-26} W m^{-2} Hz^{-1}	θ_{max} ″ arc
I	α 23^h 21^m 10·3^s δ 58° 34′ 42″	0·5	6·3	10
II	α 23^h 21^m 27·5^s δ 58° 31′ 59″	0·6	5·9	5
III	α 23^h 21^m 03·3^s δ 58° 29′ 59″	0·6	1·3	6

θ_{max} = upper limit to angular size of source from observed profile.

3.2 *Changes of structure with frequency*

The map obtained at 2695 MHz was convolved with a smoothing function so as to give it the same resolution and beam shape as the 1407 MHz map made previously by Ryle *et al.* (1965). The result is shown in Fig. 2 (i), together with the 1407 MHz map (Fig. 2 (ii)). It can be seen that the general appearance of the source has not changed markedly with frequency, although the relative strengths of the individual peaks have changed. Point to point comparison of the two maps was undertaken and after correcting for the secular decrease (Högbom & Shakeshaft 1961), which was assumed to occur uniformly for all features, values for the spectral index α for various parts of the source were derived assuming a power law of the form $S \propto \nu^{-\alpha}$ for the flux S at a frequency ν. The results are shown in Fig. 3. The errors in these values of α could be as large as $\pm 0{\cdot}2$. These results are not significantly modified by any polarization effects, since the linearly polarized component is small at both frequencies. The peaks of enhanced emission have a marked spread of values of α, and these seem unrelated to each other, although they tend to be higher on the west than on the east of the source. The broad emission shell has a fairly constant value of α of about 0·7, with the notable exceptions of the northern and south-western arcs, where gaps occur at 2695 MHz but not at 1407 MHz. Variations of spectral index across a source have been found in other supernova remnants, IC 443 (Hogg 1964; Kundu & Velusamy 1968), W 49B (Wynn-Williams 1969) and HB 21 (Erkes & Dickel 1969).

3.3 *Comparison with optical photographs*

Comparisons of the radio map with the original photograph by Baade & Minkowski (1954) and also with a recent photograph (Plate I) from the 200-inch Palomar Telescope (van den Bergh, private communication) show up a remarkable

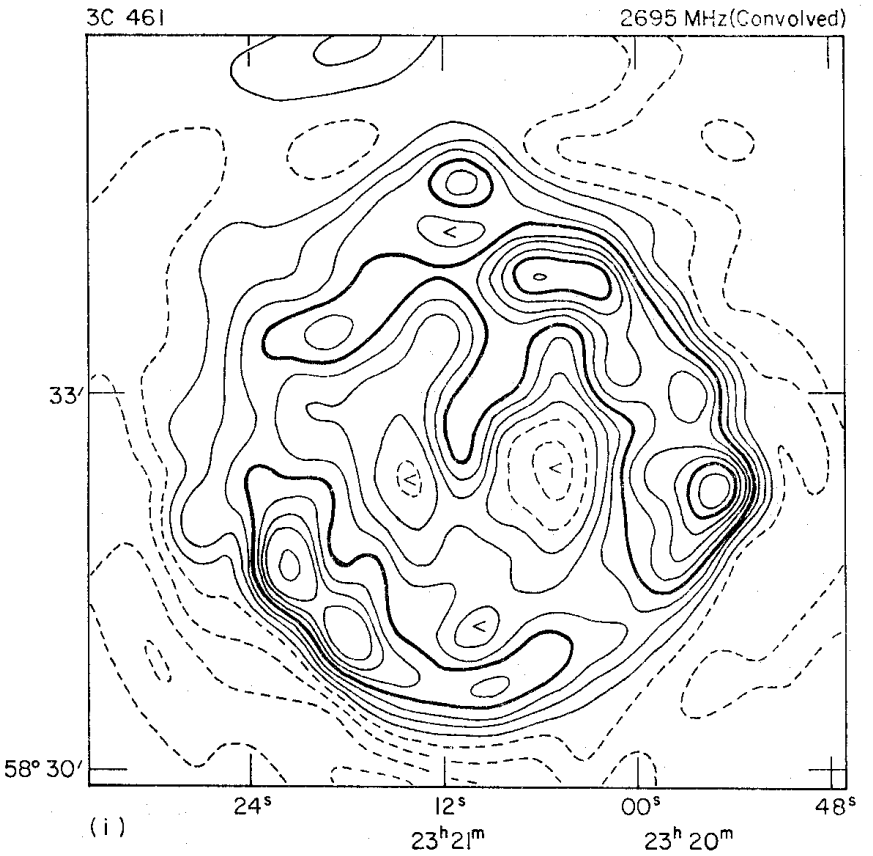

FIG. 2 (i). *Contours of Cas A at 2695 MHz after smoothing to the resolution and beamshape of the 1407 MHz map of Ryle et al.* (1965).

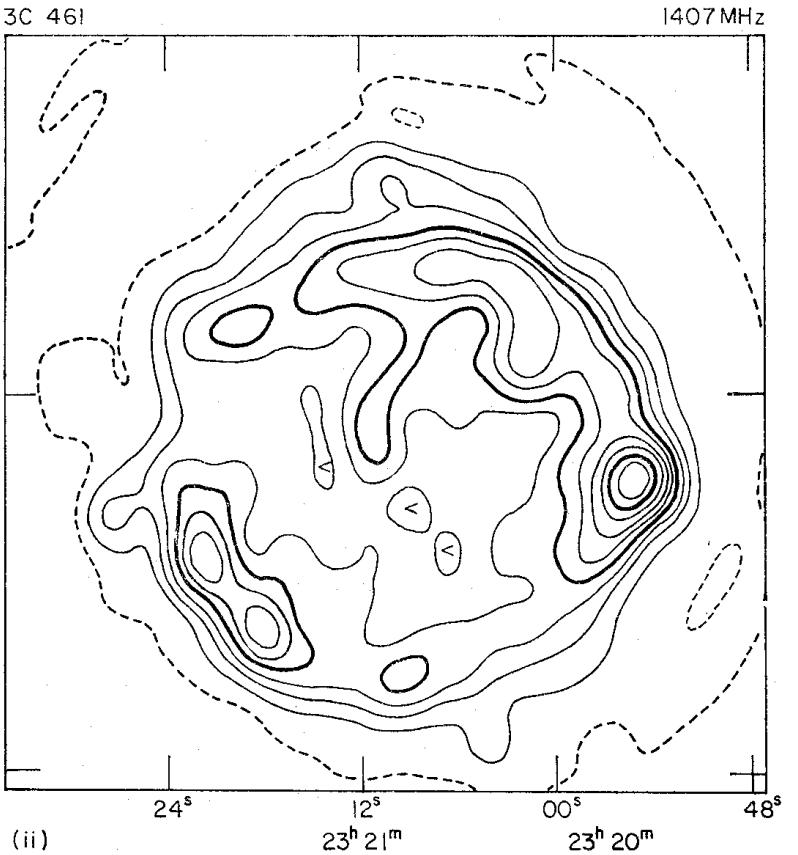

FIG. 2 (ii). *Contours of Cas A at 1407 MHz (Ryle et al. 1965) with 23″ arc resolution.*

fact. The very fast optical filaments beyond the east edge of the source, studied by Minkowski (1966) (and also mentioned by Jennison (1965)) (labelled f in Fig. 1) are not only opposite the gap in the radio shell, but are also elongated along a line at position angle 70°, almost coincident with the band of reduced radio emission mentioned in Section 3.1.5 above (Fig. 1). The filaments shaded in Fig. 1 were copied from the photograph by Baade & Minkowski (1954), where they are more clearly visible; comparison with the more recent photograph shows that the most distant flare has moved along this line. The connection between the two features is thus strongly confirmed and may stem from a preferential direction of the interstellar magnetic field, or from a band of lower interstellar gas density in that region.

All of the other nebulosities are contained within the radio contours and most of them within contour two or above. There is a large semistationary filament close to the radio feature at $\alpha \approx 23^h\ 21^m\ 20^s$, $\delta \approx 58°\ 33'\ 30''$. Diffuse filaments may also be associated with the broad peaks at $\alpha \approx 23^h\ 21^m\ 14^s$, $\delta \approx 58°\ 33'\ 50''$ and at $\alpha \approx 23^h\ 21^m\ 06^s$, $\delta \approx 58°\ 34'\ 00''$, but in general there is no detailed correspondence with other marked features. It has been pointed out by Dr D. E. Hogg (private communication) that the radio contours on the 1407 MHz map published by Ryle *et al.* (1965) are there shown about 15″ arc north of their true position. This was due to an error in the insertion of the coordinate system on that map. When corrected, the radio and optical features at the northern edge of the source are found to coincide at 1407 MHz as they do at 2695 MHz.

4. PHYSICAL CHARACTERISTICS OF THE MAIN SOURCE

4.1 *Shell parameters*

The new map of Cas A confirms that the basic structure of the source is that of a spherical shell. A circle of radius 130″ arc centred at the point $\alpha = 23^h\ 21^m\ 9{\cdot}5^s$, $\delta = 58°\ 32'\ 22''$ will pass through most of the emission peaks or include them, with the exception of the three separated compact sources. A concentric circle of radius 150″ arc, on the other hand, will pass through the latter and also include most of the low emission plateau. These circles are drawn in Fig. 3. The above point can therefore be taken as the centre of the source, with 5″ arc accuracy, and will be used as such henceforth. The declination of this centre of the radio source is in agreement, within the limits of error, with the latest estimate for the centre of expansion of the optical nebulosities (van den Bergh & Dodd 1969), but its R.A. differs by $1{\cdot}9^s \pm 0{\cdot}8^s$ (15″ ± 6″ arc) from this value. Because of the irregularities of the source, individual radial profiles have little meaning, but some estimates of the thickness and the nature of the shell were obtained by an averaging process; for each concentric annulus 10″ arc wide drawn from the centre of the source the emission was integrated and a mean contour height found which would give the same integrated flux. This procedure was carried out twice: (i) without altering the map, and (ii) after removing, by drawing a smooth line beneath them, all the peaks in the central region of the source and any structure near the edge exceeding three contours. This modified profile (ii) accounts for 88 per cent of the total emission. It was worked out to investigate whether treating the peaks separately (see Section 5) would significantly alter the values for the parameters of the shell. The resulting mean radial distributions are shown in Figs 4 (i) and 4 (ii) respectively.

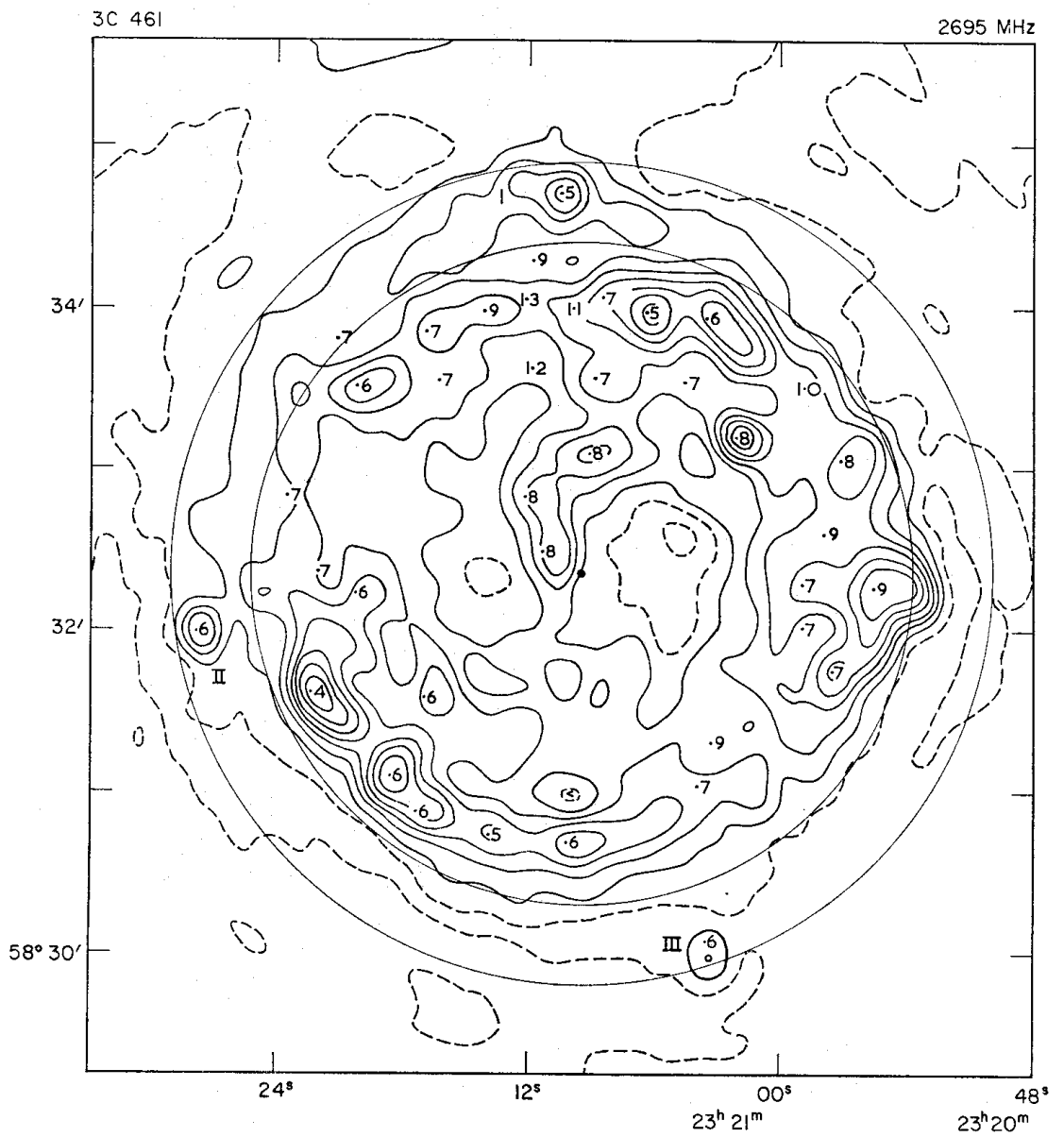

FIG. 3. *Map of distribution of spectral indices across Cas A. The two circles have* 130″ *and* 150″ *arc radius from the point shown with a dot at* $\alpha = 23^h\,21^m\,9{\cdot}5^s$, $\delta = 58°\,32'\,22''$ *(epoch* 1950.0).

4.2 *Uniform shell model*

In order to study these mean profiles a simple model, consisting of a uniform, optically thin, spherical shell, radiating isotropically, with an outer radius R and a thickness ΔR was used (Fig. 5). This model is similar to that adopted by Hill (1967).

Model profiles for various values of R and ΔR were calculated and the best fit to the outer rim of the unmodified source profile (i) was obtained for an outer radius $R = 130'' \pm 5''$ arc and a thickness $\Delta R = 30'' \pm 5''$ arc ($\Delta R/R = 0{\cdot}23$), while for the modified profile (ii) a thickness of $35'' \pm 5''$ arc ($\Delta R/R = 0{\cdot}27$) gave a better fit. These model profiles, convolved with the telescope beam, are superimposed on the histograms as continuous curves in Figs 4 (i) and 4 (ii). The

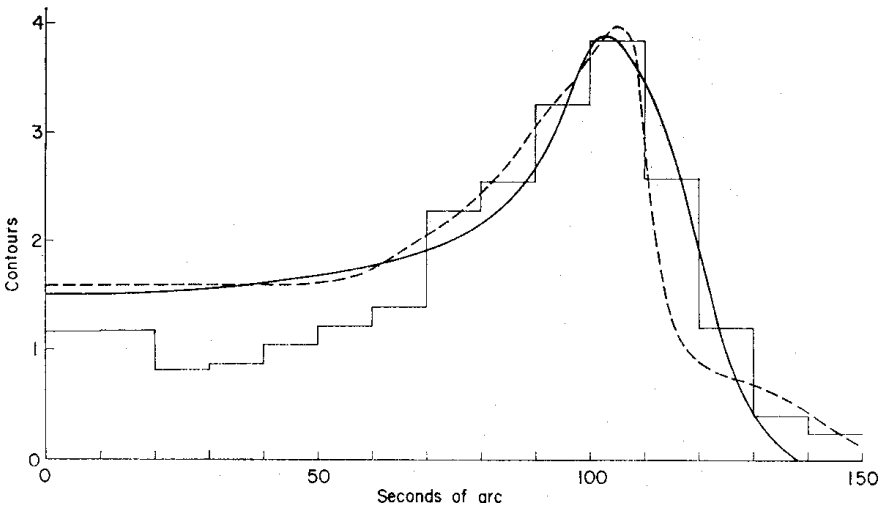

FIG. 4 (i). *The histogram is the unmodified mean profile across Cas A. The continuous and dashed curves correspond to best fit models of a single thick shell and a double shell, respectively, radiating isotropically. The derivation of these is given in the text (Section 4).*

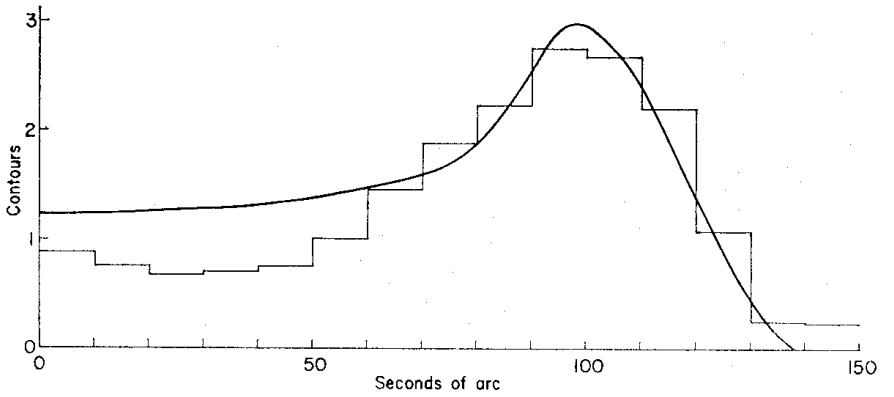

FIG. 4 (ii). *The histogram is the modified mean profile across Cas A. The continuous line corresponds to a best fit model of a thick shell radiating isotropically. The derivation is given in the text (Section 4).*

discrepancy between the predicted and observed emission from the centre of the source is discussed further in Section 4.4.

4.3 *Double shell model*

The above model, while giving a reasonably good fit to the radiation from the shell, does not account for the low emission plateau spreading beyond the edge of the shell; on the other hand, single shells reaching out to 150″ arc would not fit the ridge of the emission. This plateau could be explained in one way by postulating a leakage of energetic electrons from the source into the surrounding medium, as suggested by Baldwin (1967). Another possibility is a double shell model. This hypothesis was first put forward by Minkowski (1966) and was based on the evidence of two different spectral types among the optical filaments.

A model has been calculated using different combinations of two isotropically emitting shells and the best fit (dashed line Fig. 4 (i)) corresponds to a thick shell of outer radius 150″ ± 5″ arc and thickness 60″ ± 10″ arc together with a thin

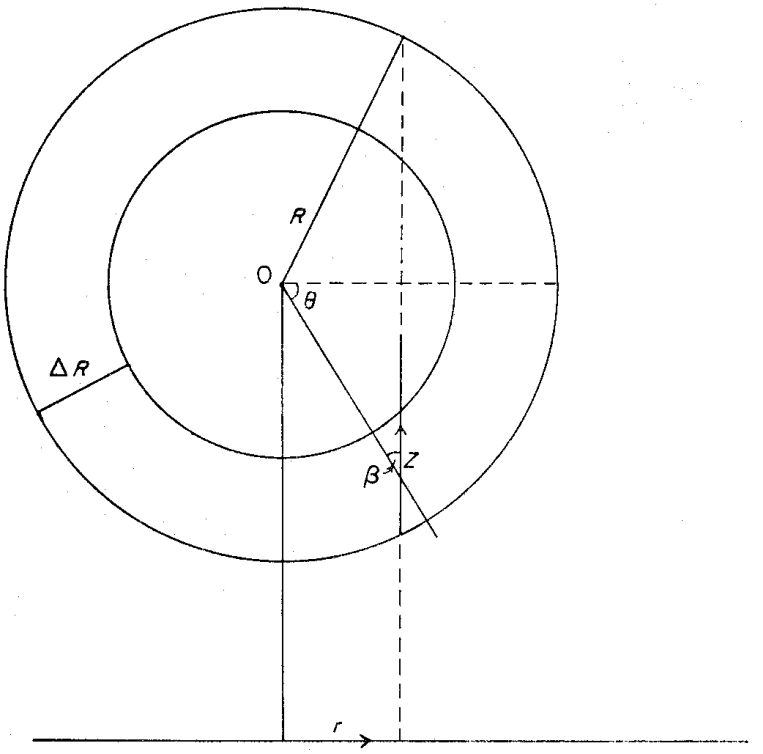

FIG. 5. *The projection of a spherical shell on to the plane of the sky.*

shell of outer radius 110″ ± 5″ arc and thickness 5″ arc. In this model the higher emission ridges, corresponding to the second shell, would contribute 35 per cent of the total flux.

4.4 *Radial magnetic field model*

The models illustrated in Figs 4 (i) and 4 (ii) predict a stronger emission from the central part of the shell than is actually observed. This discrepancy suggests that there might be preferential directions of emission from different parts of the source due to a partial alignment of the magnetic field in a radial direction throughout the expanding shell, as suggested by the results of Mayer & Hollinger (1968).

The synchrotron radiation from an isotropic, power law, electron energy distribution in a uniform magnetic field B will be linearly polarized and anisotropic, the observed intensity being proportional to $(B \sin \beta)^{\alpha+1}$ where β is the angle between the magnetic field and the line of sight and α is the spectral index as defined in the previous section; the maximum percentage of polarization observable from such a system is $(3\alpha+3)/(3\alpha+5)$ (Ginzburg & Syrovatskii 1964).

Then, for an optically thin radiating sphere of radius R the total emission integrated along a line of sight passing at a distance r from the centre will be (Fig. 5):

$$I(r) \propto \int_0^{2(R^2-r^2)^{1/2}} (B \sin \beta)^{\alpha+1}\, dz \qquad [z = (R^2-r^2)^{1/2} + r \tan \theta]$$

$$\propto \int_0^{\cos^{-1}(r/R)} r(\cos \theta)^{\alpha-1}\, d\theta \qquad \left[\beta = \frac{\pi}{2} - \theta\right]$$

$$\propto r \int_{r^2/R^2}^{1} t^{(\alpha/2)-1}(1-t)^{-1/2}\, dt \qquad [t = \cos^2 \theta].$$

This is an incomplete Beta function, for which tables are available.

The profile expected from a shell of radius $R = 130''$ arc and thickness $\Delta R = 32{\cdot}5''$ arc whose magnetic field is radially aligned has been calculated in this way for $\alpha = 0{\cdot}75$, and is shown in Fig. 6 after convolving it with the telescope beam. It can be seen that the predicted radiation from the centre of the shell is almost zero, and it clearly does not correspond to the observed emission. Also, for this value of α, a totally aligned field would produce radiation 72 per cent linearly polarized at frequencies sufficiently high for internal Faraday rotation to be negligible (see Section 4.5).

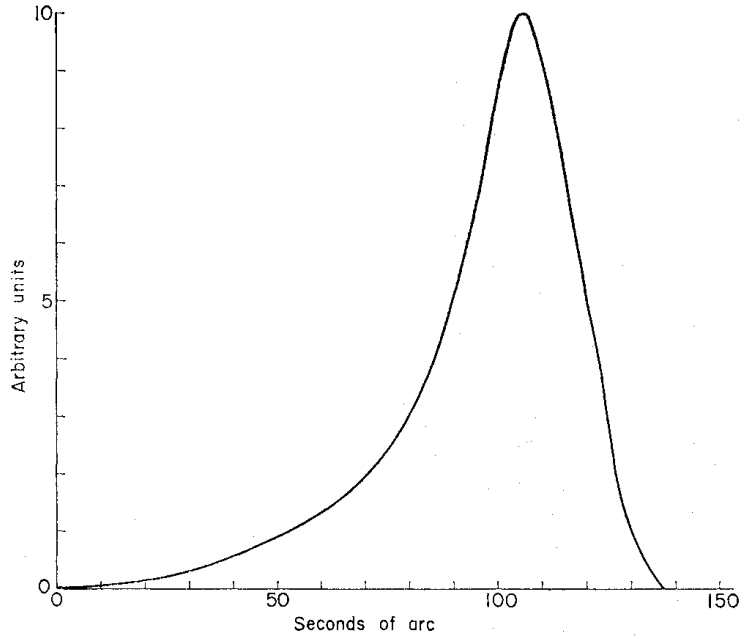

FIG. 6. *The model profile of the expected radiation from a shell with a magnetic field totally aligned in a radial direction. See text for derivation (Section 4).*

Profiles for models with partially aligned magnetic fields were calculated by adding different proportions of the totally aligned model profile of Fig. 6 to the isotropic models of Figs 4 (i) and 4 (ii). The proportions were adjusted to fit the observed emission both at the centre and at the rim of the source; the best fits were obtained with contributions of about 20 and 30 per cent for the unmodified (i) and modified (ii) mean profile, respectively.

4.5 *Polarization*

The above proportions imply values of 14 and 22 per cent, respectively, for the intrinsic linear polarization of the radiation at any point around the rim of the source. Since the amount of linear polarization at 2695 MHz is found to be less than 2 per cent the above model is only acceptable, therefore, if considerable depolarization occurs at this frequency.

The values of the density and the magnetic field strength inside the shell, estimated in Section 4.6, were used to calculate the differential Faraday rotation along the line of sight; it was assumed that the hydrogen gas in the shell was completely ionized, that the magnetic field was partially aligned as in the above model, and that the rotation occurred only within the shell. The radial alignment of the magnetic field actually decreased the rotation near the edge of the shell, and the values derived were quite insufficient to depolarize the radiation by the

required amount. The compact regions of higher magnetic field (see Section 5) which are seen around the rim of the shell will contribute to the rotation, but do not explain the small degree of polarization at all points in the map.

The Faraday rotation for both the shell and the compact components is, in any case, likely to be very small at 19 GHz and any observed polarization at that frequency cannot be much smaller than the intrinsic one. Observations by Mayer & Hollinger (1968) at 19 GHz do in fact show linearly polarized radiation around the rim of the source consistent with a radial magnetic field; the relatively small percentage polarization (average value of 4·5 per cent) is, however, incompatible with the models in Section 4.4 unless there is a change in the distribution of emission across the source at 19 GHz; it may therefore be necessary to seek an alternative explanation for the low central emission from the source. Whiteoak & Gardner (1968), for example, suggest that the low central brightness observed in a supernova remnant in Centaurus could be explained by a non-spherical model first put forward by van der Laan (1962), in which the interstellar magnetic field direction influences both the expansion of the supernova and the radiation emitted from it. The similarity in the brightness distribution between this southern source and Cas A suggests that a similar model could be applied to the latter.

4.6 *Physical parameters*

The shell fitted to the modified mean profile (ii) in Section 4.2 would have, at a distance of 3·4 kpc, an outer radius of 2·15 pc and a thickness of 0·58 pc; its volume is therefore 6×10^{56} cm^3. The flux from this shell is about 1300×10^{-26} W m^{-2} Hz^{-1} at 2695 MHz (Parker 1968) and it therefore radiates a power of $1{\cdot}4 \times 10^{17}$ W Hz^{-1} sr^{-1} at this frequency. If a value of 10 MHz is taken for the lowest frequency at which the source has a power-law spectrum, the minimum total energy for synchrotron radiation calculated from the formulae given by Ginzburg & Syrovatskii (1965) is $1{\cdot}1 \times 10^{49}$ erg, and the mean magnetic field for the minimum total energy condition is about 5×10^{-4} Gauss. This minimum energy is lower than the minimum energy which would be calculated using the volume of the whole sphere; the correct value would be slightly lower still, as some of the emission is concentrated into regions of small volume.

Minkowski (1968) has made estimates of (a) the total mass (about 2 solar masses) and (b) the density of the interstellar medium in the region of the source (about 0·2 hydrogen atoms cm^{-3}). The estimated value for the mass gives a mean density for the matter in the shell of about 5 hydrogen atoms cm^{-3}, much larger than the interstellar density. The expansion cannot therefore have been slowed down appreciably in the relatively short lifetime of the source and Minkowski (1968), combining his estimate of the ejected mass with the measured expansion velocities of the order of 7000 km s^{-1} (Minkowski 1959), derives a value for the initial kinetic energy of the expansion of 10^{51} erg, two orders of magnitudes larger than the minimum energy required in fast particles and magnetic field.

5. COMPACT REGIONS OF ENHANCED EMISSION

5.1 *Spatial distribution*

If the 25 peaks of higher emissivity shown in Fig. 1 are considered separately as being superimposed on an underlying shell (see Section 4.1), they contribute about 12 per cent to the total emission from the source. They spread out as far

as 150″ arc from the centre of the source; their density in concentric annuli drawn at 15″ arc interval from the centre of the source is plotted as a histogram in Fig. 7. An analysis of their spatial distribution shows it to be inconsistent with that of objects uniformly distributed throughout a sphere or throughout a thick shell of outer radius 150″ arc. A model distribution within a thick shell of outer radius

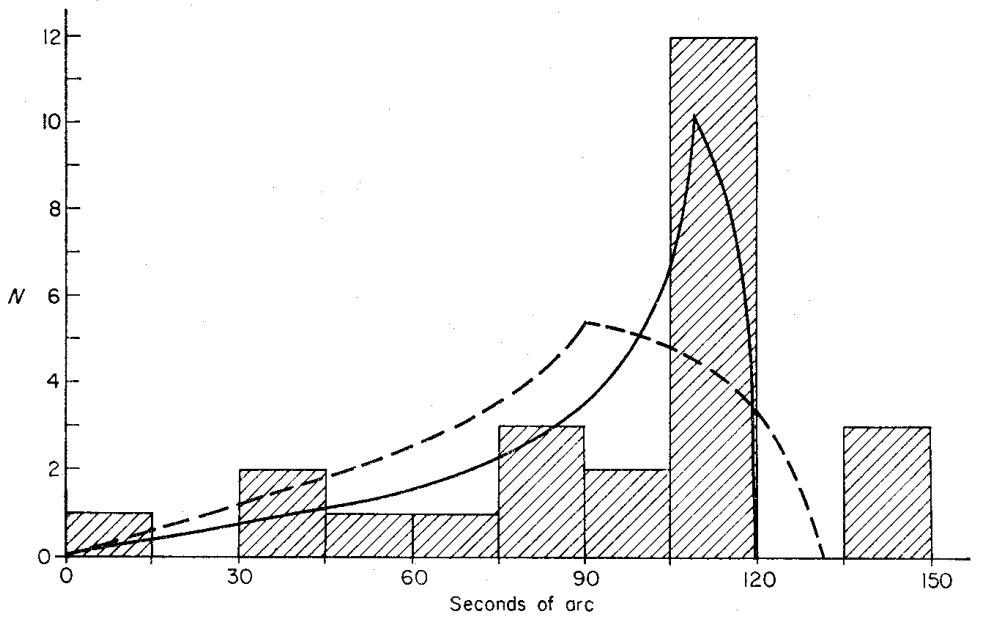

FIG. 7. *The histogram of the distribution of 25 peaks of enhanced emission across the source. The smooth lines correspond to models of uniform distribution within thin and thick shells. See text for derivations (Section 5).*

130″ arc and thickness 35″ arc (the same as the modified shell (ii) discussed in Section 4.2) gives a reasonable fit (dashed line in Fig. 7), if the three well-separated components are excluded. The best fit, however, is obtained with discrete sources distributed within a thin shell of outer radius 120″ arc and thickness 12″ arc; the expected distribution for this model is shown in Fig. 7 as a continuous curve.

5.2 *Regions within the source*

Most of the regions within the shell are to some extent confused by the main source emission, and no detailed analysis of their physical properties is immediately possible. If a flattened shape as postulated in Section 3.1.1 is assumed for these regions, however, an increase of emissivity by a factor of 10 or more with respect to the main shell source is found for most of them. This implies a higher local density of relativistic electrons or a bunching of magnetic field lines, or both; in any case some mechanism for containment of these regions is needed.

5.3 *The three separated components*

Thanks to their clear separation from the main source, the three outermost regions discussed in Section 3.1.2 can be profitably studied in detail.

Estimates of some physical quantities for these three regions have been calculated and are given in Table II. All these physical quantities can be reduced to functions of the angular diameter and the flux only, if assumptions about the method of containment of the gas clouds in the compact regions (e.g. Scheuer, in preparation), together with a further assumption of equipartition of energy between particles and magnetic field, are made. The dependence on these observable parameters is also shown in Table II.

Whenever two values are given in these tables, (a) refers to estimates derived from a containment model in which the rate of expansion of the cloud is limited by the inertia of the matter linked to the magnetic field and relativistic particles (Scheuer 1967a), and (b) refers to a model in which the gas is confined by the resistance offered by the surrounding medium through which the gas is moving (De Young & Axford 1967).

In model (a) the lifetime τ, the mass M, the radius R and the energy U of a compact source are related by the expression

$$R \approx \tau \sqrt{\frac{U}{M}}.$$

In model (b), following the calculations of Scheuer (in preparation) for an isothermal cloud, the relation between the mass M, the radius R, the energy U, the deceleration g and the relative velocity v of the gas cloud, and the density ρ of the surrounding medium are related by the expressions

$$M \approx 0{\cdot}31 \frac{U}{Rg}; \qquad U \approx 34 \rho v^2 R^3 \qquad \text{(c.g.s. units)}.$$

A value of $g = 10^{-2}$ cm s^{-2} has been used throughout the calculations, this value being an upper limit consistent with the age of the source.

Upper limits to the angular size of the three separated components can be obtained by comparing the profiles measured from the map with the known beam shape. This has been done for each region and included in Tables I and II. Estimates for a lower limit to these angular sizes were sought in observations (i) by very long baseline interferometry (Basart, Clark & Kramer 1968, with a spacing of 8×10^4 λ) and (ii) of interplanetary scintillations with the Cambridge 4·5 acre aerial (Bell 1968). These observations suggested that any structure of 1″ arc or less has a flux density $S_{2690} < 0{\cdot}6 \times 10^{-26}$ W m^{-2} Hz^{-1}, but that some structure of the order of 1–2″ arc is probably present. Since the actual sizes of these regions are not closely determined by the two limits, parameters were calculated for each region on the alternative assumptions that the upper and lower limits of angular size are the true values; these are given in Table II. The following conclusions may be drawn.

5.3.1 The estimated values of bremsstrahlung cut-off frequencies ν_{FF} derived from model (a) for angular diameters of 1″ arc or less are higher than the observing frequency, and therefore exclude the possibility of such small sizes, if this model is adopted. The values of ν_{FF} derived from model (b) for angular diameters of 1″ arc would be consistent with observations; such sizes, however, would imply emission measures so large as to make these regions very bright optical filaments, while no optical emission has been detected from them (see Plate I). The angular sizes of the three regions are therefore larger than 1″ arc, and probably 3″ arc or more.

TABLE II

Quantity	Symbol	Units		I		II		III		Dependence on θ, S, ρ_0, T	References and values
Flux density at 2695 MHz	S_{2695}	10^{-26} W m^{-2} Hz^{-1}		6·3		5·9		1·3		—	—
Spectral index	α	—		0·5		0·6		0·6		—	—
Angular diameter	θ	seconds of arc		$\theta_{max}=10$	$\theta\approx1\cdot0$	$\theta_{max}=5$	$\theta\approx1\cdot0$	$\theta_{max}=6$	$\theta\approx1\cdot0$	—	θ_{max} from present observations (Sec. 5.3)
Brightness temperature	T_b	°K		$1\cdot2\ 10^4$	$1\cdot2\ 10^6$	$4\cdot5\ 10^4$	$1\cdot1\ 10^6$	$6\cdot8\ 10^3$	$2\cdot5\ 10^5$	$\theta^{-2}\ S$	(i) p. 277
Min. energy from equipartition	U_{min}	ergs		$1\cdot4\ 10^{46}$	$7\cdot4\ 10^{44}$	$5\cdot5\ 10^{45}$	$7\cdot1\ 10^{44}$	$3\cdot0\ 10^{45}$	$3\cdot0\ 10^{44}$	$\theta^{9/7}\ S^{4/7}$	(ii) p. 305 for $\nu_{min}=10$ MHz
Magnetic field for equipartition	B	Gauss		$1\cdot3\ 10^{-3}$	$9\cdot3\ 10^{-3}$	$2\cdot0\ 10^{-3}$	$8\cdot0\ 10^{-3}$	$1\cdot1\ 10^{-3}$	$5\cdot2\ 10^{-3}$	$\theta^{-6/7}\ S^{2/7}$	From U_{min}
Mass of emitting regions	M	Solar Masses	(a)	$2\cdot0\ 10^{-3}$	$1\cdot1\ 10^{-2}$	$2\cdot7\ 10^{-3}$	$8\cdot6\ 10^{-3}$	$1\cdot0\ 10^{-3}$	$3\cdot6\ 10^{-3}$	$\theta^{-5/7}\ S^{4/7}$	(i) p. 285
		M_o hydrogen	(b)	$3\cdot9\ 10^{-4}$	$2\cdot0\ 10^{-4}$	$3\cdot6\ 10^{-4}$	$3\cdot0\ 10^{-4}$	$1\cdot6\ 10^{-4}$	$9\cdot3\ 10^{-5}$	$\theta^{2/7}\ S^{4/7}$	(iv) for $g=10^{-2}$ cm s^{-2}
Density of emitting regions	n	atoms cm^{-3}	(a)	54	$2\cdot8\ 10^5$	460	$1\cdot8\ 10^5$	100	$7\cdot7\ 10^4$	$\theta^{-26/7}\ S^{4/7}$	from Mass (a)
			(b)	9·6	$5\cdot1\ 10^3$	66	$5\cdot1\ 10^3$	16	$2\cdot0\ 10^3$	$\theta^{-19/7}\ S^{4/7}$	from Mass (b)
Faraday rotation angle at 2695 MHz	θ_F	degrees	(a)	50	$1\cdot7\ 10^5$	$4\cdot4\ 10^2$	$1\cdot4\ 10^5$	60	$3\cdot8\ 10^4$	$\theta^{-25/7}\ S^{6/7}$	(i) p. 273
			(b)	9	$3\cdot0\ 10^3$	60	$3\cdot6\ 10^3$	6	10^3	$\theta^{-18/7}\ S^{6/7}$	(i) p. 273
Velocity relative to surrounding medium needed to contain the regions in (b)	V	km s^{-1}	(b)	$1\cdot4\ 10^3$	$8\cdot2\ 10^3$	$2\cdot2\ 10^3$	$8\cdot8\ 10^3$	$1\cdot2\ 10^3$	$5\cdot5\ 10^3$	$\theta^{-6/7}\ S^{2/7}\ \rho_0^{-1/2}$	(iv) for interstellar medium density $=0\cdot1$ hydrogen atom cm^{-3}
	V	km s^{-1}	(b)	$3\cdot6\ 10^2$	$2\cdot6\ 10^3$	$7\cdot0\ 10^2$	$2\cdot8\ 10^3$	$3\cdot8\ 10^2$	$1\cdot8\ 10^3$	$\theta^{-6/7}\ S^{2/7}\ \rho_0^{-1/2}$	(iv) for interstellar medium density $=1\cdot0$ cm^{-3}
Bremsstrahlung cut-off frequency	ν_{FF}	MHz	(a)	14	$2\cdot2\ 10^4$	100	$2\cdot2\ 10^4$	32	$6\cdot2\ 10^3$	$\theta^{-3\cdot2}\ S^{4/7}\ T^{-3/4}$	(iii) p. 341 for $T=10^4$ °K
			(b)	2·5	405	12	400	3·3	170	$\theta^{-2\cdot2}\ S^{4/7}\ T^{-3/4}$	(iii) p. 341 for $T=10^4$ °K
Tsytovich cut-off frequency	ν_{TS}	MHz	(a)	0·7	510	5	500	2	330	$\theta^{-20/7}\ S^{2/7}$	(iii) p. 341
			(b)	0·1	9	0·4	9	0·2	6	$\theta^{-13/7}\ S^{2/7}$	(iii) p. 341

5.3.2 The magnitude of the derived physical quantities are not very different for regions I, II and III and may well be representative values for the remainder of the peaks.

6. SUMMARY OF RESULTS

This new high resolution map of Cas A has shown that

(a) The source has irregular and complex structure, but that most of the observed distribution of emission can be fitted by a shell of outer radius 130″ (±5″) arc and thickness 32″ (±5″) arc centred at
$$\alpha = 23^h\,21^m\,9{\cdot}5^s \pm 0{\cdot}8^s;\ \delta = 58^\circ\,32'\,22'' \pm 5''.$$
(b) Numerous intense emission regions can be distinguished, three of them being separated from the source.
(c) The association between some fast optical filaments and the main gap in the shell is confirmed.
(d) The spectral index varies across the source.
(e) The minimum energy in relativistic electrons and magnetic field is about 10^{49} erg for the main shell (the peaks of enhanced emission contribute a further energy of 10^{48} erg); this is comparable with an estimate by Burbidge (1959). Most of the energy in the supernova remnant though, is still stored in the bulk mass motion; the kinetic energy of the expanding shell is about 10^{51} erg (Minkowski 1968).

ACKNOWLEDGMENTS

The author is indebted to Professor van den Bergh for the use of his 200-inch photograph and for permission to reproduce it. He also thanks other members of the Department for valuable discussions, in particular Professor Ryle, Drs P. A. G. Scheuer, J. E. Baldwin and J. R. Shakeshaft. Many others have been involved in the observations and the reduction of data for this paper and thanks are due to them all, in particular to Messrs D. W. J. Bly, R. Atkins and L. H. Lea, who were responsible for developing the 2·7 GHz receivers with which the present observations were made, and to R. A. Hinder for providing the convolution function used to compare the two maps at different frequencies. The receipt of a University Research Maintenance Fund grant is also gratefully acknowledged.

Mullard Radio Astronomy Observatory, Cavendish Laboratory, Cambridge.

REFERENCES

Baade, W. & Minkowski, R., 1954. *Astrophys. J.*, **119**, 206.
Baldwin, J. E., 1967. I.A.U. Symposium No. 31, 337.
Basart, J. P., Clark, B. G. & Kramer, J. S., 1968. *Publ. astr. Soc. Pacific*, **80**, 273.
Bell, S. J., 1968. Ph.D. Thesis, University of Cambridge.
Braun, L. D. & Yen, J. L., 1968. *Astrophys. J.*, **153**, L 123.
Burbidge, G. R., 1959. *Paris Symposium on Radio Astronomy*, p. 541, Ed. R. N. Bracewell, Stanford University Press.
De Young, D. S. & Axford, W. I., 1967. *Nature, Lond.*, **216**, 129.
Elsmore, B., Kenderdine, S. & Ryle, M., 1966. *Mon. Not. R. astr. Soc.*, **134**, 87.
Erkes, J. W. & Dickel, J. R., 1969. *Astr. J.*, **74**, 840.

Ginzburg, V. L. & Syrovatskii, S. I., 1964. *The Origin of Cosmic Rays*, Ch. 2, Pergamon Press, Oxford.
Ginzburg, V. L. & Syrovatskii, S. I., 1965. *A. Rev. Astr. Astrophys.*, **3**, 297.
Hill, E. R., 1967. *Aust. J. Phys.*, **20**, 297.
Hobbs, R. W. & Haddock, F. T., 1967. *Astrophys. J.*, **147**, 908.
Hobbs, R. W., Corbert, H. H. & Santini, N. J., 1968. *Astrophys. J.*, **152**, 43.
Hobbs, R. W. & Hollinger, J. P., 1968. *Astrophys. J.*, **154**, 423.
Högbom, J. A. & Shakeshaft, J. R., 1961. *Nature, Lond.*, **189**, 561.
Hogg, D. E., 1964. *Astrophys. J.*, **140**, 992.
Hollinger, J. P. & Hobbs, R. W., 1968. *Astrophys. J.*, **151**, 771.
Jennison, R. C., 1965. *Nature, Lond.*, **207**, 740.
Kesteven, M. J. L., 1968. *Aust. J. Phys.*, **21**, 739.
Kundu, M. R. & Velusamy, T., 1968. *Mon. Not. R. astr. Soc.*, **140**, 173.
Mayer, C. H. & Hollinger, J. P., 1968. *Astrophys. J.*, **151**, 53.
Minkowski, R., 1959. *Paris Symposium on Radio Astronomy*, p. 315, Ed. R. N. Bracewell, Stanford University Press.
Minkowski, R., 1966. *Nature, Lond.*, **209**, 1339.
Minkowski, R., 1968. *Non-Thermal Galactic Sources*, Ch. 11 of *Nebulae and Interstellar Gas*, Eds. B. Middlehurst & L. Aller, University of Chicago Press.
Parker, E. A., 1968. *Mon. Not. R. astr. Soc.*, **138**, 407.
Pooley, G. G. & Ryle, M., 1968. *Mon. Not. R. astr. Soc.*, **139**, 515.
Ryle, M., 1962. *Nature, Lond.*, **194**, 517.
Ryle, M., Elsmore, B. & Neville, A. C., 1965. *Nature, Lond.*, **205**, 1259.
Scheuer, P. A. G., 1967a. Chapter on *Radio Galaxies and QSS* in *Plasma Astrophysics*, Ed. P. A. Sturrock, Academic Press, London.
Scheuer, P. A. G., 1967b. Chapter on *Radiation* in *Plasma Astrophysics*, Ed. P. A. Sturrock, Academic Press, London.
Scheuer, P. A. G. & Williams, P. J. S., 1968. *A. Rev. Astr. Astrophys.*, **6**, 321.
Seielstad, G. A. & Weiler, K. W., 1968. *Astrophys. J.*, **154**, 817.
van den Bergh, S. & Dodd, W. W., 1969. *Nature, Lond.*, **223**, 814.
van der Laan, H., 1962. *Mon. Not. R. astr. Soc.*, **124**, 179.
Whiteoak, J. B. & Gardner, F. F., 1968. *Astrophys. J.*, **154**, 807.
Wynn-Williams, C. G., 1969. *Mon. Not. R. astr. Soc.*, **142**, 453.